

Parameter-space metric of semicoherent searches for continuous gravitational waves

Holger J. Pletsch*

*Max-Planck-Institut für Gravitationsphysik (Albert-Einstein-Institut) and
Leibniz Universität Hannover, Callinstraße 38, D-30167 Hannover, Germany*

(Dated: 15:33, Thursday 25th October, 2018)

Continuous gravitational-wave (CW) signals such as emitted by spinning neutron stars are an important target class for current detectors. However, the enormous computational demand prohibits fully coherent broadband all-sky searches for prior unknown CW sources over wide ranges of parameter space and for yearlong observation times. More efficient hierarchical “semicoherent” search strategies divide the data into segments much shorter than one year, which are analyzed coherently; then detection statistics from different segments are combined incoherently. To optimally perform the incoherent combination, understanding of the underlying parameter-space structure is requisite. This problem is addressed here by using new coordinates on the parameter space, which yield the first analytical parameter-space metric for the incoherent combination step. This semicoherent metric applies to broadband all-sky surveys (also embedding directed searches at fixed sky position) for isolated CW sources. Furthermore, the additional metric resolution attained through the combination of segments is studied. From the search parameters (sky position, frequency, and frequency derivatives), solely the metric resolution in the frequency derivatives is found to significantly increase with the number of segments.

PACS numbers: 04.80.Nn, 95.55.Ym, 95.75.-z, 97.60.Gb

I. INTRODUCTION

Direct detection of gravitational waves would not only validate Einstein’s theory of general relativity but also constitute an important new astronomical tool. Continuous gravitational-wave (CW) signals are expected, for instance, from rapidly rotating neutron stars through various emission mechanisms [1–5]. Most such stars are anticipated to be electromagnetically invisible, but might be detected and studied via gravitational waves. With current Earth-based detectors, such as LIGO [6], numerous efforts are underway to search for CW sources [7–10], and observational upper limits have already allowed one to constrain the physics of neutron stars [11, 12].

The expected CW signals are extremely weak. Hence detection requires very sensitive data analysis techniques to extract these signals from detector noise. In the work of [13] a powerful method has been derived which is based on the principle of maximum likelihood detection, leading to coherent matched filtering. The CW signals are quasimonochromatic with a slowly changing intrinsic frequency. For a terrestrial detector, the Earth’s motion relative to the solar system barycenter (SSB) generates a Doppler modulation in amplitude and phase of the waveform. As shown in [13], the parameters describing the signal’s amplitude variation may be analytically eliminated by maximizing the coherent matched-filtering statistic. Thus, one only searches over the remaining parameters describing the signal’s phase: the source’s sky location, frequency, and frequency derivatives (“spindowns”). The so-obtained coherent detection statistic is called the \mathcal{F} -statistic, which can also be generalized to employ multiple detector data streams [14].

Finite computational resources are what imposes severe

limits on the sensitivity of broadband all-sky searches for prior unknown CW sources [13, 15]. In the fully coherent \mathcal{F} -statistic approach, one must convolve the full data set with signal waveforms (templates) corresponding to all possible sources. But the number of templates required to cover the search parameter space increases as a high power of the coherent integration time. For year-long data sets, searching a realistic range of parameter space would demand more computing power than available on Earth [13, 15]. Therefore, a fully coherent search is restricted to much shorter integration times.

A more efficient analysis of data sets which span yearlong time intervals is achieved via less expensive hierarchical semicoherent methods [16–19]. In such a method, the data are divided into segments of duration T , where T is much smaller than one year. This allows one to use a *coarse* grid of templates, on which the \mathcal{F} -statistic is calculated for each segment. Then the \mathcal{F} -statistics from all segments (or statistics derived from \mathcal{F}) are incoherently combined using a common *fine* grid of templates. Since phase information is discarded between segments, this latter step is called incoherent and thus the search methodology as a whole is referred to as *semicoherent*.

An important long-standing problem in these semicoherent methods has been the design of, and link between, the coarse and fine grids. To address this problem it is essential to understand the underlying parameter-space structure. In this context, the geometric approach has been proven to be very useful, introducing a *metric* on parameter space, as first done in [20, 21]. The key quantity in this respect is called *mis-match* \mathcal{M} , which is the fractional loss in expected \mathcal{F} -statistic (or sum of expected \mathcal{F} -statistics in the incoherent step) for a given signal \mathbf{p}_{sig} at a nearby grid point \mathbf{p} in phase-parameter space \mathcal{P} . Taylor-expanding \mathcal{M} (to quadratic order) at \mathbf{p}_{sig} in the differences of \mathbf{p}_{sig} and \mathbf{p} defines the parameter-space metric.

While the parameter-space metric for coherent searches has

*Electronic address: Holger.Pletsch@aei.mpg.de

been examined in detail [15, 22, 23], the metric for semicoherent searches is comparably much less well studied. However, the literature does exhibit several quests for a semicoherent metric [17, 18, 24, 25]. About a decade ago, the first general discussion of the semicoherent metric for CW searches was given in [16], along with numerical investigations. But only recently, the first fully analytical semicoherent metric has been found, leading to a significantly improved CW search method [19]. This recent progress is based on a better understanding of the global parameter-space correlations [26], which were first examined in [27]. In turn, this insight provides new coordinates on parameter space, enabling the analytical calculation and study of the semicoherent metric.

The present paper extends the recent work of [19] to greater generality and provides the essential technical basis for a parameter-space metric formalism for semicoherent CW searches. Additionally, complete and fully analytic semicoherent metric results are presented, which are ready to use for practical implementations of semicoherent searches, serving the earlier-mentioned quests of previous literature. The results apply to broadband all-sky surveys (embedding directed searches with fixed sky position) for isolated CW sources.

Section II briefly reviews matched filtering for CW signals and the parameter-space metric formalism in general. Section III elucidates how the metric is obtained for semicoherent searches. To evaluate and study the semicoherent metric, new coordinates on parameter space are defined in Sec. IV. In Sec. V, the semicoherent metric is derived and investigated for the case of CW signals whose intrinsic frequency changes linearly with time (parametrized by one spindown parameter). In particular, the refinement factor is introduced as the ratio of the number fine-grid and coarse-grid templates, quantifying the additional parameter-space metric resolution due to combination of many segments. Section VI extends these results to the case of CW signals whose intrinsic frequency can change quadratically with time (considering two spindown parameters). Finally, a short conclusion follows in Sec. VII.

II. MATCHED FILTERING FOR CONTINUOUS GRAVITATIONAL-WAVE SIGNALS

The detector output data time series is denoted by $x(t)$ at detector time t . In the absence of any signal, the data contain only noise $n(t)$, which is assumed to be a zero-mean, stationary, and Gaussian random process. In case a signal $h(t)$ is present, the noise is assumed to be additive, such that $x(t) = n(t) + h(t)$.

The dimensionless signal response function $h(t)$ of an interferometric detector to a weak plane gravitational wave in the long-wavelength approximation is a linear combination of the form

$$h(t) = F_+(t) h_+(t) + F_\times(t) h_\times(t), \quad (1)$$

where $F_{+,\times}$ are called the beam-pattern functions, resulting in the amplitude modulations from Earth's spinning motion. They lie in the range $-1 \leq F_{+,\times} \leq 1$, and depend on the orientation of the detector and source, and on the polarization

angle ψ of the waves. For explicit expressions the reader is referred to [13]. In the case of an isolated rapidly rotating neutron star with nonaxisymmetric deformations and negligible proper motion (cf. [28, 29]), the waveforms corresponding to the plus (+) and cross (\times) polarizations are

$$h_+(t) = A_+ \sin \Psi(t), \quad h_\times(t) = A_\times \cos \Psi(t), \quad (2)$$

where A_+ and A_\times are the plus and cross polarization amplitude parameters, respectively, and $\Psi(t)$ is given by

$$\begin{aligned} \Psi(t) &= \Phi_0 + \Phi(t) \\ &= \Phi_0 + 2\pi \sum_{k=0}^s \frac{f^{(k)}(t_0)}{(k+1)!} \left[t - t_0 + \frac{\vec{r}(t) \cdot \vec{n}}{c} \right]^{k+1}, \end{aligned} \quad (3)$$

where Φ_0 is the initial phase, $f^{(0)} \equiv f$ denotes the frequency, and $f^{(k>0)}$ is the k th frequency time derivative (also called ‘‘spindown’’), evaluated at the SSB at time t_0 . The integer $s > 0$ denotes the number of frequency time derivatives to be taken into account, therefore it holds $f^{(k>s)} = 0$. The vector $\vec{r}(t)$ connects from the SSB to the detector, c is the speed of light, and \vec{n} is a constant unit vector pointing from the SSB to the location of the CW source. Thus, a point in phase parameter space $\mathbf{p} \in \mathcal{P}$ is denoted by $\mathbf{p} = (f^{(k)}, \vec{n})$ in respect of the reference time t_0 .

As first shown in [13], the phase $\Phi(t)$ in Eq. (3) can be approximated without significant loss in signal-to-noise ratio (SNR) to good accuracy by

$$\begin{aligned} \Phi(t) &\approx 2\pi \sum_{k=0}^s \frac{f^{(k)}(t_0) (t - t_0)^{k+1}}{(k+1)!} \\ &\quad + 2\pi \frac{\vec{r}(t)}{c} \cdot \vec{n} \sum_{k=0}^s \frac{f^{(k)}(t_0) (t - t_0)^k}{k!}. \end{aligned} \quad (4)$$

Consider a data segment spanning the interval $[-T/2, T/2]$. The \mathcal{F} -statistic is obtained [13, 30] from the likelihood ratio Λ , which takes the form

$$\ln \Lambda = (x|h) - \frac{1}{2}(h|h), \quad (5)$$

where the scalar product has been defined as

$$(x|y) \equiv 4\Re \int_0^\infty \frac{\tilde{x}(f) \tilde{y}^*(f)}{S_n(f)} df, \quad (6)$$

with the Fourier transform indicated by $\tilde{}$, the complex conjugation denoted by $*$, and S_n defined as the one-sided noise spectral density. One may assume S_n to be constant over the narrow bandwidth of the signal considered in this work. Then the scalar product of Eq. (6) is approximately given by

$$(x|y) \approx \frac{2}{S_n} \int_{-T/2}^{T/2} x(t) y(t) dt. \quad (7)$$

Thus, the time average is introduced by the following notation:

$$\langle x \rangle \equiv \frac{1}{T} \int_{-T/2}^{T/2} x(t) dt. \quad (8)$$

Using this notation, Eq. (5) is rewritten as

$$\ln \Lambda = \frac{2T}{S_n} \left[\langle x h \rangle - \frac{1}{2} \langle h^2 \rangle \right]. \quad (9)$$

Replacing the amplitude parameters $\{A_+, A_\times, \psi, \Phi_0\}$ by their values which maximize $\ln \Lambda$, the so-called maximum likelihood (ML) estimators, defines the detection statistic \mathcal{F} as

$$\mathcal{F} \equiv \ln \Lambda_{\text{ML}}. \quad (10)$$

Because the \mathcal{F} -statistic is maximized over the amplitude parameters, the remaining search space is just the phase-parameter space \mathcal{P} .

A. Coherent detection statistic for a simplified signal model

Since the primary goal of this work is in relation to template-grid construction, a very useful approximation for this purpose is to replace the beam-pattern functions $F_{+,\times}(t)$ by constant values [26, 28, 31]. The phase of the CW signal is expected to change very rapidly at the terrestrial detector site over a time scale of typically less than ten seconds, whereas the amplitude of the signal varies with a period of one sidereal day. Coherent observation times of practical interest are typically longer than one day, so that replacing the beam-pattern functions $F_{+,\times}(t)$ with effective constant values is a good approximation. In this case the signal model in Eq. (1) takes the form

$$h(t) = A_1 \sin \Phi(t) + A_2 \cos \Phi(t), \quad (11)$$

where $A_{1,2}$ are defined to be the constant amplitude parameters. In [28], the validity of this approximation is also investigated using Monte Carlo simulations. It should be noted that the actual computation of the \mathcal{F} -statistic in a CW search will, of course, include the effects of amplitude modulation and involves precise calculation of the detector position with respect to the SSB using an accurate ephemeris model. This simplified signal is used here to facilitate the template-grid construction.

The log likelihood of Eq. (9) for the simplified signal model (11) is denoted by $\ln \Lambda^*$ and takes the form

$$\ln \Lambda^* = \frac{2T}{S_n} \left[A_1 \langle x \sin \Phi \rangle + A_2 \langle x \cos \Phi \rangle - \frac{A_1^2 + A_2^2}{4} \right]. \quad (12)$$

By substituting the ML estimators for $A_{1,2}$ in $\ln \Lambda^*$ of Eq. (12), it is straightforward to show [26, 27] that the simplified signal model (11) leads to the following coherent detection statistic \mathcal{F}^* approximating \mathcal{F} as

$$\mathcal{F}^* = \ln \Lambda_{\text{ML}}^* = \frac{2T}{S_n} \left| \langle x e^{-i\Phi} \rangle \right|^2. \quad (13)$$

B. Perfect match of signal and template phase parameters

Consider a signal $h_{\text{sig}}(t)$ following the model of Eq. (11) present in the data $x(t)$. Let the signal's phase evolution

$\Phi_{\text{sig}}(t)$ be described by *known* phase parameters denoted by the vector \mathbf{p}_{sig} and defined at t_0 ,

$$h_{\text{sig}}(t) = A_{1,\text{sig}} \sin \Phi_{\text{sig}}(t) + A_{2,\text{sig}} \cos \Phi_{\text{sig}}(t). \quad (14)$$

Since the signal parameters are known, one can construct a template which perfectly matches the signal. Assuming the noise $n(t)$ to be stationary, Gaussian, zero-mean, and additive, one can show [32, 33] that for a known signal (zero parameter offsets) the expectation value and variance of \mathcal{F}^* , respectively, are

$$E[\mathcal{F}^*] = 1 + \frac{1}{2} \rho^2(0), \quad \sigma_{\mathcal{F}^*}^2 = 1 + \rho^2(0), \quad (15)$$

where $\rho(0)$ defines the optimal SNR, obtained as

$$\rho^2(0) = \frac{4T}{S_n} \left| \langle h_{\text{sig}} e^{-i\Phi_{\text{sig}}} \rangle \right|^2. \quad (16)$$

The expression of Eq. (16) may be further simplified using Eq. (14) to yield

$$\rho^2(0) = \frac{T}{S_n} (A_{1,\text{sig}}^2 + A_{2,\text{sig}}^2). \quad (17)$$

C. Mismatch of the signal and template phase parameters

If the signal parameters are *unknown* in advance, one has to evaluate the detection statistic for a bank of templates. Let the template phase-parameter vector be \mathbf{p} and the corresponding phase be $\Phi(t)$. In general, the template phase parameters will not exactly match the signal parameters. Thus, the parameter offsets are labeled by

$$\Delta \mathbf{p} \equiv \mathbf{p}_{\text{sig}} - \mathbf{p}. \quad (18)$$

The resulting difference in phase $\Delta \Phi(t)$ between the phase $\Phi_{\text{sig}}(t)$ of the signal and the phase $\Phi(t)$ of a template is defined as

$$\Delta \Phi(t) \equiv \Phi_{\text{sig}}(t) - \Phi(t). \quad (19)$$

In this case the expectation value and variance of \mathcal{F}^* , respectively, are given by

$$E[\mathcal{F}^*] = 1 + \frac{1}{2} \rho^2(\Delta \mathbf{p}), \quad \sigma_{\mathcal{F}^*}^2 = 1 + \rho^2(\Delta \mathbf{p}) \quad (20)$$

where the SNR $\rho(\Delta \mathbf{p})$ here depends on the parameter offsets $\Delta \mathbf{p}$, such that

$$\rho^2(\Delta \mathbf{p}) = \frac{4T}{S_n} \left| \langle h_{\text{sig}} e^{-i\Phi} \rangle \right|^2. \quad (21)$$

Further simplification of Eq. (21) leads to

$$\begin{aligned} \rho^2(\Delta \mathbf{p}) &= \frac{T}{S_n} (A_{1,\text{sig}}^2 + A_{2,\text{sig}}^2) \left| \langle e^{i\Delta \Phi} \rangle \right|^2 \\ &= \rho^2(0) \left| \langle e^{i\Delta \Phi} \rangle \right|^2. \end{aligned} \quad (22)$$

The above relation shows that given an offset $\Delta \mathbf{p}$ between the signal and template parameters the squared SNR is reduced by $|\langle e^{i\Delta\Phi} \rangle|^2$. This gives rise to define a dimensionless ‘‘mismatch’’ \mathcal{M} as

$$\mathcal{M} = \frac{\rho^2(0) - \rho^2(\Delta \mathbf{p})}{\rho^2(0)} \quad (23a)$$

$$= 1 - |\langle e^{i\Delta\Phi} \rangle|^2. \quad (23b)$$

The mismatch represents the fractional loss in the expected detection statistic due to the parameter $\Delta \mathbf{p}$ and thus provides a distance measure in the template parameter space.

D. Metric on parameter space

Taylor-expanding the mismatch \mathcal{M} up to quadratic order in terms of the template parameter-space location offsets \mathbf{p} at the signal location \mathbf{p}_{sig} yields

$$\mathcal{M} \approx \sum_{a,b} g_{ab} \Delta \mathbf{p}^a \Delta \mathbf{p}^b, \quad (24)$$

defining a positive definite metric tensor g as

$$g_{ab} = \langle \partial_a \Phi \partial_b \Phi \rangle - \langle \partial_a \Phi \rangle \langle \partial_b \Phi \rangle, \quad (25)$$

where a and b label the tensor indices, and the following notation has been employed:

$$\partial_a \Phi \equiv \left. \frac{\partial \Phi}{\partial \mathbf{p}^a} \right|_{\mathbf{p}=\mathbf{p}_{\text{sig}}}. \quad (26)$$

The expression of Eq. (25) is often called the ‘‘phase metric’’ [15, 23, 29], since it describes a distance measure on the phase parameter space \mathcal{P} .

III. PARAMETER-SPACE METRIC FOR SEMICOHERENT SEARCHES

In semicoherent CW searches the data are divided into N segments of duration T , where T is much smaller than one year. This allows to analyze each segment coherently, using a *coarse* grid of templates. Then the coherent detection statistic results from all segments are incoherently combined using a common *fine* grid of templates. This scheme is often called a semicoherent search strategy, offering the best overall sensitivity at limited computational resources [16, 17] when the fully coherent approach is infeasible. In preparation of calculating the semicoherent metric, this section introduces some general notation.

A. The coherent metric for a given segment

Let the integer $j = 1, \dots, N$ label the j th segment, and let t_j denote the time midpoint of segment j . The time average over

the j th segment is defined by

$$\langle x \rangle_{[j]} \equiv \frac{1}{T} \int_{t_j-T/2}^{t_j+T/2} x(t) dt. \quad (27)$$

The mismatch \mathcal{M}_j in the j th segment is given by

$$\mathcal{M}_j = \frac{\rho^2(0) - \rho_j^2(\Delta \mathbf{p})}{\rho^2(0)}, \quad (28)$$

where

$$\rho_j^2(\Delta \mathbf{p}) = \rho^2(0) |\langle e^{i\Delta\Phi} \rangle_{[j]}|^2. \quad (29)$$

Thus \mathcal{M}_j can be approximated by

$$\mathcal{M}_j \approx \sum_{a,b} g_{ab}^{[j]} \Delta \mathbf{p}^a \Delta \mathbf{p}^b, \quad (30)$$

where the components of coherent metric tensor for the j th segment $g^{[j]}$ are obtained in analogy to Eq. (25) as

$$g_{ab}^{[j]} = \langle \partial_a \Phi \partial_b \Phi \rangle_{[j]} - \langle \partial_a \Phi \rangle_{[j]} \langle \partial_b \Phi \rangle_{[j]}. \quad (31)$$

When searching a subspace $\mathcal{S}_{\mathcal{P}}$ of the phase parameter space \mathcal{P} , the corresponding proper volume V is given by

$$V = \int_{\mathcal{S}_{\mathcal{P}}} dV = \int_{\mathcal{S}_{\mathcal{P}}} \sqrt{\det g^{[j]}} d\mathbf{p}. \quad (32)$$

The placement of signal templates to cover the search parameter space is an instance of the sphere covering problem [34]. Using a lattice of templates, the number of coarse-grid templates $\mathcal{N}_t^{\text{coarse}}$ is obtained from the coherent metric tensor $g^{[j]}$ as

$$\mathcal{N}_t^{\text{coarse}} = \rho_0 V = \rho_0 \int_{\mathcal{S}_{\mathcal{P}}} \sqrt{\det g^{[j]}} d\mathbf{p}, \quad (33)$$

where the constant ρ_0 describes the density of templates. The specific value of ρ_0 depends on the desired maximum mismatch and the chosen type of lattice [15, 32, 34]. When using a random template bank instead of a lattice, then ρ_0 can also depend on the desired coverage fraction [35, 36].

B. The semicoherent metric for combining segments

In the semicoherent search approach, coherent detection statistic results from the different segments are incoherently combined. To evaluate the metric for this case, the simplified coherent detection statistic \mathcal{F}^* (approximating \mathcal{F}) of Eq. (13) is again used here. Thus, \mathcal{F}_j^* means the \mathcal{F}^* -statistic value obtained in the j th segment. Recall that \mathcal{F}_j^* is the log likelihood function (maximized over the amplitude parameters). As the joint likelihood is the product, the joint log likelihood of all segments is the sum over j . Therefore, we define the semicoherent detection statistic $\overline{\mathcal{F}}^*$ by

$$\overline{\mathcal{F}}^* = \frac{1}{N} \sum_{j=1}^N \mathcal{F}_j^*. \quad (34)$$

For the case of a known signal (zero parameter offsets) the expectation value and variance of $\overline{\mathcal{F}^*}$, respectively, are

$$E[\overline{\mathcal{F}^*}] = 1 + \frac{1}{2}\rho^2(0), \quad \sigma_{\overline{\mathcal{F}^*}}^2 = \frac{1 + \rho^2(0)}{N}, \quad (35)$$

assuming identical noise spectral densities S_n in every segment. Hence, combining detection statistics from the N segments reduces the variance by N .

For nonzero offsets $\Delta\mathbf{p}$ between the template and signal parameters the resulting expectation value and variance of $\overline{\mathcal{F}^*}$, respectively, are obtained as

$$E[\overline{\mathcal{F}^*}] = 1 + \frac{1}{2N} \sum_{j=1}^N \rho_j^2(\Delta\mathbf{p}), \quad (36)$$

$$\sigma_{\overline{\mathcal{F}^*}}^2 = \frac{1 + \frac{1}{N} \sum_{j=1}^N \rho_j^2(\Delta\mathbf{p})}{N}. \quad (37)$$

Thus, the mismatch $\overline{\mathcal{M}}$, which measures the fractional loss in the expected semicoherent detection statistic $\overline{\mathcal{F}^*}$ due to phase-parameter offsets $\Delta\mathbf{p}$ is obtained as

$$\begin{aligned} \overline{\mathcal{M}} &= \frac{1}{N} \sum_{j=1}^N \frac{\rho^2(0) - \rho_j^2(\Delta\mathbf{p})}{\rho^2(0)} \\ &= \frac{1}{N} \sum_{j=1}^N \mathcal{M}_j. \end{aligned} \quad (38)$$

Since \mathcal{M}_j is the mismatch in segment j according to Eq. (30), $\overline{\mathcal{M}}$ represents the average mismatch across the segments (cf. [16]). Consequently, one may write

$$\overline{\mathcal{M}} \approx \sum_{a,b} \bar{g}_{ab} \Delta\mathbf{p}^a \Delta\mathbf{p}^b, \quad (39)$$

where the components of the semicoherent metric tensor \bar{g} are obtained as the average of the individual-segment coherent metric components $g_{ab}^{[j]}$ from Eq. (31),

$$\bar{g}_{ab} = \frac{1}{N} \sum_{j=1}^N g_{ab}^{[j]}. \quad (40)$$

Thus, in analogy to Eq. (33) the number of fine-grid templates $\mathcal{N}_t^{\text{fine}}$ is given by

$$\mathcal{N}_t^{\text{fine}} = \rho_0 \int_{\mathcal{S}_{\mathcal{P}}} \sqrt{\det \bar{g}} \, d\mathbf{p}. \quad (41)$$

IV. NEW COORDINATES ON PARAMETER SPACE

The standard ‘‘physical’’ coordinates on \mathcal{P} are the frequency and frequency derivatives $f^{(k)}(t_0)$ at reference time t_0 , and the unit vector $\vec{n} = (\cos \delta \cos \alpha, \cos \delta \sin \alpha, \sin \delta)$ on the two-sphere S^2 , pointing from the SSB to the source. The angles α and δ are right ascension and declination.

The analytic evaluation of the semicoherent metric components \bar{g}_{ab} from Eq. (40) is one of the central aspects of this work. This problem is approached by introducing new coordinates on the phase parameter space \mathcal{P} , leading to a phase model which depends linearly on the coordinates.

A. Linear phase model

For coherent segment lengths T much smaller than one year, the orbital component \vec{r}_{orb} of the Earth’s motion, $\vec{r} = \vec{r}_{\text{orb}} + \vec{r}_{\text{spin}}$, varies slowly during T and thus can be Taylor expanded around the segment’s midpoint. Hence, by separating the orbital and spinning components of the Earth’s motion in the phase model $\Phi(t)$ a convenient reparameterization is obtained in which $\Phi(t)$ depends linearly on the new coordinates. For further details the reader is referred to Ref. [26]. Thus the resulting phase model $\Phi(t)$ is obtained as

$$\begin{aligned} \Phi(t) &= \phi_0(t_0) + \sum_{k=0}^s \nu^{(k)}(t_0) \left(\frac{t - t_0}{T} \right)^{k+1} 2^{k+1} \\ &\quad + n_x(t_0) \cos \Omega t + n_y(t_0) \sin \Omega t, \end{aligned} \quad (42)$$

where $\phi_0(t_0)$ is a constant independent of t , and the new frequency and frequency-derivative coordinates $\nu^{(k)}(t_0)$ as first derived in [26] are

$$\begin{aligned} \nu^{(k)}(t_0) &\equiv 2\pi \left(\frac{T}{2} \right)^{k+1} \left[\frac{f^{(k)}(t_0)}{(k+1)!} \right. \\ &\quad \left. + \sum_{\ell=0}^{k+1} \frac{f^{(\ell)}(t_0)}{\ell!(k-\ell+1)!} \vec{\xi}^{(k-\ell+1)}(t_0) \cdot \vec{n} \right], \end{aligned} \quad (43)$$

and the new sky coordinates (as in [19, 31]) are given by

$$n_x(t_0) \equiv 2\pi f(t_0) \tau_E \cos \delta_D \cos \delta \cos[\alpha - \alpha_D(t_0)], \quad (44a)$$

$$n_y(t_0) \equiv 2\pi f(t_0) \tau_E \cos \delta_D \cos \delta \sin[\alpha - \alpha_D(t_0)]. \quad (44b)$$

Thereby, $\vec{\xi}(t) \equiv \vec{r}_{\text{orb}}(t)/c$, with $\vec{r}_{\text{orb}}(t)$ denoting the vector from the Earth’s barycenter to the SSB, and, $\tau_E = R_E/c \approx 21$ ms is the light travel time from the Earth’s center to the detector, $\alpha_D(t_0)$, δ_D are the detector position at time t_0 , and $\Omega = 2\pi/(1 \text{ sd})$ is the angular velocity of the Earth’s spinning motion, which has a period of one sidereal day.

Apart from an overall factor, the quantities $\nu^{(k)}$ have been referred to as the ‘‘global-correlation parameters’’ [19, 26]. As similarly done in earlier work [23, 31], note that the parameters $\nu^{(k)}$ include a rescaling factor of $(T/2)^{k+1}$, such that they become dimensionless for convenience.

B. Validity estimation

The phase model of Eq. (42) is an approximation to the phase evolution described by Eq. (4). The validity of this approximation depends on the coherent integration time T

(duration of a given segment) and on the source frequencies searched, as was previously investigated in [26, 31]. The maximum value of T as a function of the highest search frequency f may be estimated by considering the first neglected term in the phase model becomes large enough to eventually lead to a significant mismatch. Given the phase model of Eq. (42) and searching s spindown parameters, the first neglected term $\Delta\phi_s$ is given by

$$\Delta\phi_s(t) \equiv 2\pi \frac{(t-t_0)^{s+2}}{(s+2)!} f(t_0) \vec{\xi}^{(s+2)}(t_0) \cdot \vec{n} \quad (45)$$

$$\leq 2\pi \frac{(t-t_0)^{s+2}}{(s+2)!} f(t_0) \left| \vec{\xi}^{(s+2)}(t_0) \right|. \quad (46)$$

The mismatch produced by the phase offset $\Delta\phi_s$ follows from Eq. (28) as $1 - |\langle e^{i\Delta\phi_s} \rangle|^2$. Figure 1 shows the values of T as a function of frequency f for which $\Delta\phi_s$ yields a mismatch of 30%. For instance, with $s = 1$, one should be able to use coherent segment durations T up to about 2 days for search frequencies f up to about 1kHz, such that the mismatch due to the approximate phase model of Eq. (42) is still less than about 30%. These results also qualitatively agree with the earlier investigations reported in [31].

However, most importantly, the new coordinates $\{\nu^{(k)}, n_x, n_y\}$ have significant advantages over the original coordinates $\{f^{(k)}, \vec{n}\}$. These new coordinates permit the first analytical solution for the metric of the incoherent combination step in hierarchical searches, yielding the ‘‘semi-coherent metric’’ to be presented in the following. In addition, in these new coordinates, the obtained metric is explicitly coordinate independent, a very convenient feature when it comes to practical aspects of conducting CW searches.

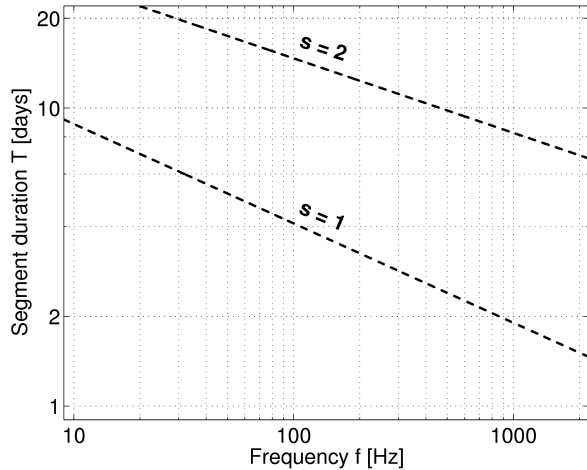


FIG. 1: Validity estimation of the approximate phase model Eq. (42) in terms of the number of spindown parameters s considered, for given values of coherent integration time T and the source frequencies searched. The dashed lines correspond to 30% mismatch for the one and two spindown case, respectively. For example, when including one spindown parameter ($s = 1$), the mismatch due to the approximate phase model should be less than 30% for coherent integrations T up to about 2 days while searching frequencies up to about 1kHz.

V. METRIC EVALUATION FOR ONE SPINDOWN PARAMETER

For all-sky surveys of prior unknown CW sources the search parameter space \mathcal{S}_P is typically a four-dimensional subspace of \mathcal{P} [7–9, 12], restricting to linear changes in frequency (one spindown parameter). In this case, using the new coordinates a point in \mathcal{P} is labeled by the vector $\mathbf{p} = (\nu, \dot{\nu}, n_x, n_y)$ at a given reference time t_0 . The phase model of Eq. (42) with $s = 1$ takes the form

$$\Phi(t) = \phi_0(t_0) + \nu(t_0) \frac{2(t-t_0)}{T} + \dot{\nu}(t_0) \frac{4(t-t_0)^2}{T^2} + n_x(t_0) \cos \Omega t + n_y(t_0) \sin \Omega t, \quad (47)$$

where the coordinates ν and $\dot{\nu}$ from Eq. (43) are explicitly written as

$$\nu(t_0) = 2\pi \frac{T}{2} \left[f(t_0) + f(t_0) \dot{\xi}(t_0) \cdot \vec{n} + \dot{f} \xi(t_0) \cdot \vec{n} \right], \quad (48a)$$

$$\dot{\nu}(t_0) = 2\pi \left(\frac{T}{2} \right)^2 \left[\dot{f} + \frac{f(t_0)}{2} \ddot{\xi}(t_0) \cdot \vec{n} + \dot{f} \dot{\xi}(t_0) \cdot \vec{n} \right]. \quad (48b)$$

The coordinates n_x and n_y are as given by Eqs. (44).

A. Coherent metric

Using the coordinates $\{\nu, \dot{\nu}, n_x, n_y\}$, the components $g_{ab}^{[j]}$ of the symmetric coherent metric tensor can be computed analytically from Eq. (31). Thereby it is useful to define the dimensionless quantity φ as

$$\varphi \equiv \Omega \frac{T}{2}. \quad (49)$$

Thus from Eq. (31) the components $g_{ab}^{[j]}$ are obtained as

$$g_{\nu\nu}^{[j]} = \frac{1}{3}, \quad (50a)$$

$$g_{\nu\dot{\nu}}^{[j]} = \frac{4}{3} \left(\frac{t_j - t_0}{T} \right), \quad (50b)$$

$$g_{\dot{\nu}\dot{\nu}}^{[j]} = \frac{4}{45} + \frac{16}{3} \left(\frac{t_j - t_0}{T} \right)^2, \quad (50c)$$

$$g_{\nu n_x}^{[j]} = -j_1(\varphi) \sin(\Omega t_j), \quad (50d)$$

$$g_{\nu n_y}^{[j]} = j_1(\varphi) \cos(\Omega t_j), \quad (50e)$$

$$g_{\dot{\nu} n_x}^{[j]} = -\frac{2}{3} j_2(\varphi) \cos(\Omega t_j) - 4 j_1(\varphi) \left(\frac{t_j - t_0}{T} \right) \sin(\Omega t_j), \quad (50f)$$

$$g_{\dot{\nu} n_y}^{[j]} = -\frac{2}{3} j_2(\varphi) \sin(\Omega t_j) + 4 j_1(\varphi) \left(\frac{t_j - t_0}{T} \right) \cos(\Omega t_j), \quad (50g)$$

$$g_{n_x n_x}^{[j]} = \frac{1}{2} - \frac{1}{2} j_0(\varphi) \cos(\varphi) - j_1(\varphi) \sin(\varphi) \cos^2(\Omega t_j), \quad (50h)$$

$$g_{n_x n_y}^{[j]} = -j_1(\varphi) \sin(\varphi) \sin(\Omega t_j) \cos(\Omega t_j), \quad (50i)$$

$$g_{n_y n_y}^{[j]} = \frac{1}{2} - \frac{1}{2} j_0(\varphi) \cos(\varphi) - j_1(\varphi) \sin(\varphi) \sin^2(\Omega t_j), \quad (50j)$$

where the spherical Bessel functions $j_n(x)$ [37] are defined by

$$j_n(x) \equiv (-x)^n \left(\frac{1}{x} \frac{d}{dx} \right)^n \frac{\sin(x)}{x}. \quad (51)$$

The first few spherical Bessel functions are given by

$$j_0(x) = \frac{\sin(x)}{x}, \quad (52a)$$

$$j_1(x) = \frac{\sin(x)}{x^2} - \frac{\cos(x)}{x}, \quad (52b)$$

$$j_2(x) = \left[\frac{3}{x^2} - 1 \right] \frac{\sin(x)}{x} - \frac{3 \cos(x)}{x^2}, \quad (52c)$$

$$j_3(x) = \left[\frac{15}{x^3} - \frac{6}{x} \right] \frac{\sin(x)}{x} - \left[\frac{15}{x^2} - 1 \right] \frac{\cos(x)}{x}. \quad (52d)$$

Note that the components $g_{ab}^{[j]}$ of the coherent metric tensor are *explicitly independent* of the coordinates. Therefore, the number of coarse-grid templates $\mathcal{N}_t^{\text{coarse}}$ as described by Eq. (33) can be rewritten as

$$\mathcal{N}_t^{\text{coarse}} = \rho_0 \sqrt{\det g^{[j]}} \int_{\mathcal{S}_P} d\mathbf{p}, \quad (53)$$

where $\sqrt{\det g^{[j]}}$ has been taken outside the integration over the searched region of parameter space, since it is independent of the coordinates. Thus, $\sqrt{\det g^{[j]}}$ directly scales the number of templates $\mathcal{N}_t^{\text{coarse}}$. The actual value of $\mathcal{N}_t^{\text{coarse}}$ depends on the parameter-space region \mathcal{S}_P searched over. To analytically obtain realistic estimates for $\mathcal{N}_t^{\text{coarse}}$, one may assume the ranges

$$\pi T f_{\min} \lesssim \nu \lesssim \pi T f_{\max}, \quad (54)$$

$$-\pi \frac{T^2 f}{4 \tau_{\min}} \lesssim \dot{\nu} \lesssim \pi \frac{T^2 f}{4 \tau_{\min}}, \quad (55)$$

where $\tau_{\min} = f/\dot{f}$ represents the ‘‘minimum spindown age’’ [13] to search for. At fixed frequency f the parameter ranges of n_x and n_y determine a two-dimensional disk \mathcal{D}_f with radius of about $2\pi f \tau_E$. Thus, Eq. (53) yields

$$\begin{aligned} \mathcal{N}_t^{\text{coarse}} &= \rho_0 \sqrt{\det g^{[j]}} \\ &\times \int_{\pi T f_{\min}}^{\pi T f_{\max}} d\nu \int_{\mathcal{D}_f} dn_x dn_y \int_{-\frac{\pi T^2 f}{4 \tau_{\min}}}^{\frac{\pi T^2 f}{4 \tau_{\min}}} d\dot{\nu} \\ &\approx \rho_0 \sqrt{\det g^{[j]}} \frac{\pi^5 \tau_E^2}{2 \tau_{\min}} T^3 (f_{\max}^4 - f_{\min}^4). \end{aligned} \quad (56)$$

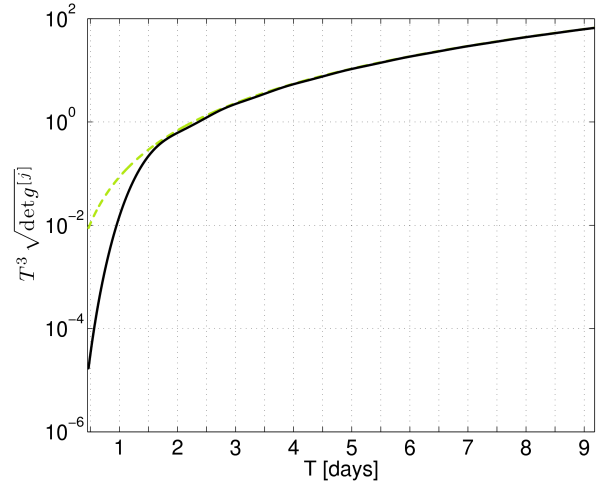


FIG. 2: Dependency of the number of coarse-grid templates $\mathcal{N}_t^{\text{coarse}}$ on the coherent integration time T (segment length) for the one-spindown case. The solid curve shows $T^3 \sqrt{\det g^{[j]}}$, since $\mathcal{N}_t^{\text{coarse}} \propto T^3 \sqrt{\det g^{[j]}}$. The dashed curve represents $T^3/\sqrt{135}$.

The determinant of the coherent metric tensor $\det g^{[j]}$ is obtained as

$$\begin{aligned} \det g^{[j]} &= \frac{1}{135} [1 - 6 j_1^2(\varphi) - j_0(\varphi) \cos(\varphi)] \\ &\times [1 - 10 j_2^2(\varphi) - j_1(\varphi) \sin(\varphi) \\ &\quad - j_0(\varphi) \cos(\varphi)]. \end{aligned} \quad (57)$$

Note that $\det g^{[j]}$ is also explicitly independent of the reference time t_0 (as well as of t_j), and solely depends upon φ . This can be understood from the following reasoning. For the parameters $f^{(k)}$ a change of reference time corresponds to a linear transformation [28, 29], whose determinant is 1. Similarly, for the parameters n_x and n_y a change of reference time can be described by a rotation, whose determinant is also 1. Therefore this explains why $\det g^{[j]}$ is independent of the reference time.

To examine the scaling of $\mathcal{N}_t^{\text{coarse}}$ with the coherent integration time T , Fig. 2 shows $T^3 \sqrt{\det g^{[j]}}$, which is a measure for $\mathcal{N}_t^{\text{coarse}}$, as a function of T . For increasing values of T , $\det g^{[j]}$ converges to $1/135$, since the metric tensor components related to the Earth’s spinning motion, n_x and n_y , become approximately constant. This behavior can be understood from the Rayleigh criterion. An estimate of the diffraction-limited resolution is described by the ratio of the wavelength and the effective ‘‘baseline’’ [23]. The maximum baseline in terms of the Earth’s spinning motion is the Earth’s diameter, which is first reached already after half a day of integration. Therefore, very little metric resolution is gained after integration times T of about a day, as long as the Earth’s orbital motion can still be well modeled by a Taylor expansion.

Finally, it should be mentioned that a convenient choice of t_0 in favor of a compact notation is $t_0 = t_j = 0$. To indicate this choice has been made, the resulting coherent metric tensor is denoted by $g^{[j=0]}$. The components $g_{ab}^{[j=0]}$ are obtained

from Eqs. (50) as follows:

$$g_{\nu\nu}^{[j=0]} = \frac{1}{3}, \quad (58a)$$

$$g_{\nu\dot{\nu}}^{[j=0]} = 0, \quad (58b)$$

$$g_{\dot{\nu}\dot{\nu}}^{[j=0]} = \frac{4}{45}, \quad (58c)$$

$$g_{\nu n_x}^{[j=0]} = 0, \quad (58d)$$

$$g_{\nu n_y}^{[j=0]} = j_1(\varphi), \quad (58e)$$

$$g_{\dot{\nu} n_x}^{[j=0]} = -\frac{2}{3} j_2(\varphi), \quad (58f)$$

$$g_{\dot{\nu} n_y}^{[j=0]} = 0, \quad (58g)$$

$$g_{n_x n_x}^{[j=0]} = \frac{1}{2} - \frac{1}{2} j_0(\varphi) \cos(\varphi) - j_1(\varphi) \sin(\varphi), \quad (58h)$$

$$g_{n_x n_y}^{[j=0]} = 0, \quad (58i)$$

$$g_{n_y n_y}^{[j=0]} = \frac{1}{2} - \frac{1}{2} j_0(\varphi) \cos(\varphi). \quad (58j)$$

B. Semicoherent metric

Given the coherent metric tensor components $g_{ab}^{[j]}$ in Eqs. (50), explicit expressions for the components \bar{g}_{ab} of the semicoherent metric tensor \bar{g} are obtained via Eq. (40) as

$$\bar{g}_{\nu\nu} = \frac{1}{3}, \quad (59a)$$

$$\bar{g}_{\nu\dot{\nu}} = \frac{4}{3} \mu_1, \quad (59b)$$

$$\bar{g}_{\dot{\nu}\dot{\nu}} = \frac{4}{45} + \frac{16}{3} \mu_2, \quad (59c)$$

$$\bar{g}_{\nu n_x} = -j_1(\varphi) \mu_0^{\text{SIN}}, \quad (59d)$$

$$\bar{g}_{\nu n_y} = j_1(\varphi) \mu_0^{\text{COS}}, \quad (59e)$$

$$\bar{g}_{\dot{\nu} n_x} = -\frac{2}{3} j_2(\varphi) \mu_0^{\text{COS}} - 4 j_1(\varphi) \mu_1^{\text{SIN}}, \quad (59f)$$

$$\bar{g}_{\dot{\nu} n_y} = -\frac{2}{3} j_2(\varphi) \mu_0^{\text{SIN}} + 4 j_1(\varphi) \mu_1^{\text{COS}}, \quad (59g)$$

$$\bar{g}_{n_x n_x} = \frac{1}{2} - \frac{1}{2} j_0(\varphi) \cos(\varphi) - j_1(\varphi) \sin(\varphi) \zeta_2^{\text{COS}}, \quad (59h)$$

$$\bar{g}_{n_x n_y} = -j_1(\varphi) \sin(\varphi) \zeta_1^{\text{SINCOS}}, \quad (59i)$$

$$\bar{g}_{n_y n_y} = \frac{1}{2} - \frac{1}{2} j_0(\varphi) \cos(\varphi) - j_1(\varphi) \sin(\varphi) \zeta_2^{\text{SIN}}, \quad (59j)$$

using the following notations to simplify the expressions:

$$\mu_m \equiv \frac{1}{N} \sum_{j=1}^N \left(\frac{t_j - t_0}{T} \right)^m, \quad (60)$$

$$\mu_m^{\text{SIN}} \equiv \frac{1}{N} \sum_{j=1}^N \left(\frac{t_j - t_0}{T} \right)^m \sin(\Omega t_j), \quad (61)$$

$$\mu_m^{\text{COS}} \equiv \frac{1}{N} \sum_{j=1}^N \left(\frac{t_j - t_0}{T} \right)^m \cos(\Omega t_j), \quad (62)$$

$$\zeta_2^{\text{SIN}} \equiv \frac{1}{N} \sum_{j=1}^N \sin^2(\Omega t_j), \quad \zeta_2^{\text{COS}} \equiv \frac{1}{N} \sum_{j=1}^N \cos^2(\Omega t_j), \quad (63)$$

$$\zeta_1^{\text{SINCOS}} \equiv \frac{1}{N} \sum_{j=1}^N \sin(\Omega t_j) \cos(\Omega t_j), \quad (64)$$

where m can be zero or a positive integer number.

The components \bar{g}_{ab} of the semicoherent metric tensor are also explicitly independent of the coordinates. Therefore, the number of fine-grid templates $\mathcal{N}_t^{\text{fine}}$ as described by Eq. (41) is rewritten as

$$\begin{aligned} \mathcal{N}_t^{\text{fine}} &= \rho_0 \sqrt{\det \bar{g}} \int_{\mathcal{S}_p} d\mathbf{p} \\ &= \mathcal{N}_t^{\text{coarse}} \sqrt{\frac{\det \bar{g}}{\det g^{[j]}}}. \end{aligned} \quad (65)$$

Considering the distribution of the segments' midpoints $\{t_j\}$, the quantities μ_m may be interpreted as the m th moment of this distribution. Thus a very convenient choice of reference time t_0 for the semicoherent metric is given by the time average of all segment's midpoints $\{t_j\}$,

$$t_0 = \frac{1}{N} \sum_{j=1}^N t_j. \quad (66)$$

With this choice of t_0 the quantities μ_m become the m th central moments (denoted by $\hat{\mu}_m$) of the distribution of the segment midpoints $\{t_j\}$.

In addition, for a large number of segments N , where the data set spans over many cycles of the Earth's spinning motion with the one-day period $2\pi/\Omega$, the following approximations may also be used:

$$\frac{1}{N} \sum_{j=1}^N \sin(\Omega t_j) \approx 0, \quad \frac{1}{N} \sum_{j=1}^N \cos(\Omega t_j) \approx 0, \quad (67a)$$

$$\frac{1}{N} \sum_{j=1}^N \sin^2(\Omega t_j) \approx \frac{1}{2}, \quad \frac{1}{N} \sum_{j=1}^N \cos^2(\Omega t_j) \approx \frac{1}{2}, \quad (67b)$$

$$\frac{1}{N} \sum_{j=1}^N \sin(\Omega t_j) \cos(\Omega t_j) \approx 0, \quad (67c)$$

as well as

$$\frac{1}{N} \sum_{j=1}^N \frac{t_j}{T} \sin(\Omega t_j) \approx 0, \quad \frac{1}{N} \sum_{j=1}^N \frac{t_j}{T} \cos(\Omega t_j) \approx 0. \quad (67d)$$

Hence, given $\mu_0^{\text{SIN}} \approx 0$, $\mu_0^{\text{COS}} \approx 0$, $\mu_1^{\text{SIN}} \approx 0$, $\mu_1^{\text{COS}} \approx 0$, $\zeta_2^{\text{SIN}} \approx 1/2$, $\zeta_2^{\text{COS}} \approx 1/2$, and $\zeta_1^{\text{SINCOS}} \approx 0$, the semicoherent metric components of Eqs. (59) along with the t_0 choice of Eq. (66) take the following *diagonal* form:

$$\bar{g} \approx \begin{pmatrix} \frac{1}{3} & 0 & 0 & 0 \\ 0 & \frac{4}{45} + \frac{16}{3} \hat{\mu}_2 & 0 & 0 \\ 0 & 0 & \frac{R(\varphi)}{2} & 0 \\ 0 & 0 & 0 & \frac{R(\varphi)}{2} \end{pmatrix}, \quad (68)$$

where $R(\varphi)$ is defined as

$$R(\varphi) \equiv 1 - j_0(\varphi) \cos(\varphi) - j_1(\varphi) \sin(\varphi). \quad (69)$$

The determinant of the above semicoherent metric tensor \bar{g}_{ab} from Eq. (68) is obtained as

$$\det \bar{g} \approx \left[\frac{1}{135} + \frac{4}{9} \hat{\mu}_2 \right] R^2(\varphi). \quad (70)$$

Finally, if T is an integer multiple q of one sidereal day, $T = \frac{2\pi}{\Omega} q$, such that $\varphi = \pi q$ and $R(\pi q) = 1$, the metric tensor \bar{g} from Eqs. (68) simplifies to

$$\bar{g} \approx \begin{pmatrix} \frac{1}{3} & 0 & 0 & 0 \\ 0 & \frac{4}{45} + \frac{16}{3} \hat{\mu}_2 & 0 & 0 \\ 0 & 0 & \frac{1}{2} & 0 \\ 0 & 0 & 0 & \frac{1}{2} \end{pmatrix}, \quad (71)$$

and the corresponding determinant is simply given by

$$\det \bar{g} \approx \frac{1}{135} + \frac{4}{9} \hat{\mu}_2. \quad (72)$$

C. Parameter-space resolution refinement

The results for the semicoherent metric tensor shown in Eqs. (68) feature an important property: $\bar{g}_{\nu\nu}$ represents the *only* component of the semicoherent metric tensor \bar{g} which significantly changes with an increased number of data segments N , not converging to some constant value. In this respect, increasing N means that the number of fine-grid templates needs to be increased in only one dimension compared to a given coarse grid.

To describe the refinement quantitatively, we use Eq. (65) to introduce the *refinement factor*, denoted by γ , defining the ratio of the fine and coarse template-grid points:

$$\gamma \equiv \frac{\mathcal{N}_t^{\text{fine}}}{\mathcal{N}_t^{\text{coarse}}} = \sqrt{\frac{\det \bar{g}}{\det g^{[j]}}, \quad (73)$$

where in the last step Eqs. (53) and (65) have been used. In what follows, refinement factor γ_1 (γ_2) with the subscript 1 (2) is used to indicate the one-spindown (two-spindown) case, respectively.

Thus, by means of Eqs. (57) and (70) the refinement factor γ_1 for the one-spindown case is explicitly given by

$$\gamma_1 = \sqrt{1 + 60 \hat{\mu}_2} Q(\varphi), \quad (74)$$

where the function $Q(\varphi)$ is defined as

$$Q(\varphi) \equiv R(\varphi) [1 - 6 j_1^2(\varphi) - j_0(\varphi) \cos(\varphi)]^{-1/2} \\ \times [1 - 10 j_2^2(\varphi) - j_1(\varphi) \sin(\varphi) \\ - j_0(\varphi) \cos(\varphi)]^{-1/2}. \quad (75)$$

Note that from Eq. (74) it is obvious that γ_1 scales linearly with the number of data segments N , since only $\hat{\mu}_2$ depends (quadratically) on N . Hence, the enhanced parameter-space resolution resulting from the incoherent combination increases approximately as $\propto N$ solely due to the first spindown parameter. This is related to the fact that the number of possible (linear) spindown tracks in frequency across all segments, of course, grows linearly with N , too.

D. Illustrative example

As for a simple example, one may consider the case where N segments are uniformly distributed in such a way that there are no gaps between neighboring segments, so that $t_j = [j - (N + 1)/2] T$. It should be pointed out that this special case had been assumed *a priori* in the previous work of [16]. Thus, for this particular instance the numerical findings of [16] can be compared to the analytic results found here. Denote the time span of the entire data set as $T_{\text{data}} \equiv N T$. Thus, in the present example the choice of Eq. (66) yields $t_0 = 0$ and

$$\hat{\mu}_2 = \frac{N^2 - 1}{12}. \quad (76)$$

For this case, γ_1 is shown in Fig. 3 for different values of T and N . For increasing values of T , γ_1 rapidly converges to some upper-limit value for fixed N . This maximum constant value can be arrived at analytically in the following way. In this regime of T , $\det g^{[j]}$ from Eq. (57) can be approximated by $1/135$ and $\det \bar{g}$ by Eq. (72), leading to $Q(\varphi) \approx 1$ in Eq. (74) and thus

$$\gamma_1 \approx \sqrt{1 + 60 \hat{\mu}_2} = \sqrt{5N^2 - 4}. \quad (77)$$

where Eq. (76) has been used in the latter step. This result agrees well with the corresponding refinement factor that can be computed from the numerical template counting formulas given in [16].

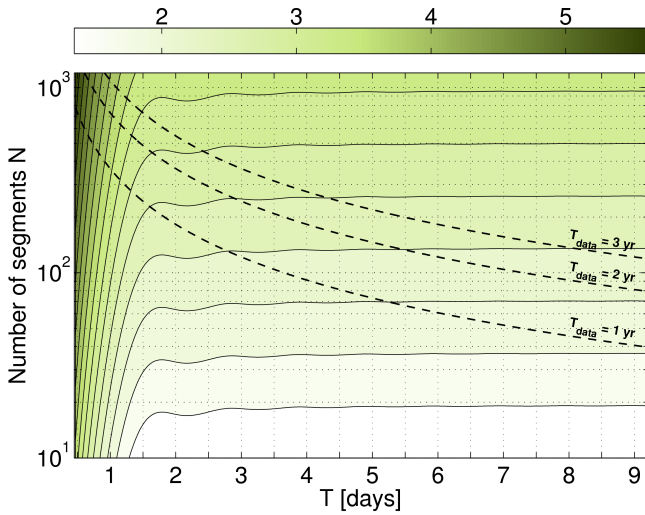


FIG. 3: Refinement factor γ_1 for the one-spindown case. In this plot the color-coded contours show $\log_{10}(\gamma_1)$ as a function of the coherent segment length T and the number of segments N . It has been assumed that there are no gaps between neighboring segments, and so Eq. (76) has been used. The dashed lines mark locations of data sets with total time span ($T_{\text{data}} = NT$) of one, two, and three years.

VI. METRIC EVALUATION FOR TWO SPINDOWN PARAMETERS

Searching for CW signals from potentially younger objects, spinning down faster, might eventually require one to also include a second spindown parameter (see [38] for an example), taking also into account quadratic changes in frequency with time. In this section, the additional semicoherent metric components are computed, which arise when a second spindown parameter is included in the search. Thus, the coordinates $\{\nu, \dot{\nu}, \ddot{\nu}, n_x, n_y\}$ at time t_0 are used to label a point in this five-dimensional parameter space. The phase model of Eq. (42) with $s = 2$ is given by

$$\begin{aligned} \Phi(t) = & \phi_0(t_0) + \nu(t_0) \frac{2(t-t_0)}{T} + \dot{\nu}(t_0) \frac{4(t-t_0)^2}{T^2} \\ & + \ddot{\nu}(t_0) \frac{8(t-t_0)^3}{T^3} + n_x(t_0) \cos \Omega t + n_y(t_0) \sin \Omega t. \end{aligned} \quad (78)$$

Based on Eq. (43) the coordinates ν , $\dot{\nu}$, and $\ddot{\nu}$ are explicitly written as

$$\begin{aligned} \nu(t_0) = & 2\pi \frac{T}{2} \left[f(t_0) + f(t_0) \dot{\xi}(t_0) \cdot \vec{n} \right. \\ & \left. + \dot{f}(t_0) \xi(t_0) \cdot \vec{n} \right], \end{aligned} \quad (79a)$$

$$\begin{aligned} \dot{\nu}(t_0) = & 2\pi \left(\frac{T}{2} \right)^2 \left[\frac{\dot{f}(t_0)}{2} + \frac{f(t_0)}{2} \ddot{\xi}(t_0) \cdot \vec{n} \right. \\ & \left. + \dot{f}(t_0) \dot{\xi}(t_0) \cdot \vec{n} + \frac{\dot{f}}{2} \xi(t_0) \cdot \vec{n} \right], \end{aligned} \quad (79b)$$

$$\begin{aligned} \ddot{\nu}(t_0) = & 2\pi \left(\frac{T}{2} \right)^3 \left[\frac{\ddot{f}}{6} + \frac{f(t_0)}{6} \ddot{\xi}(t_0) \cdot \vec{n} \right. \\ & \left. + \frac{\dot{f}(t_0)}{2} \ddot{\xi}(t_0) \cdot \vec{n} + \frac{\dot{f}}{2} \dot{\xi}(t_0) \cdot \vec{n} \right]. \end{aligned} \quad (79c)$$

The coordinates n_x and n_y are as introduced in Eqs. (44).

A. Coherent metric

Including a second spindown parameter $\ddot{\nu}$ in the phase model of Eq. (42) yields the following additional components for the coherent metric tensor $g^{[j]}$:

$$g_{\nu\dot{\nu}}^{[j]} = \frac{1}{5} + 4 \left(\frac{t_j - t_0}{T} \right)^2, \quad (80a)$$

$$g_{\dot{\nu}\dot{\nu}}^{[j]} = \frac{4}{3} \left(\frac{t_j - t_0}{T} \right) + 16 \left(\frac{t_j - t_0}{T} \right)^3, \quad (80b)$$

$$g_{\dot{\nu}\ddot{\nu}}^{[j]} = \frac{1}{7} + 8 \left(\frac{t_j - t_0}{T} \right)^2 + 48 \left(\frac{t_j - t_0}{T} \right)^4, \quad (80c)$$

$$\begin{aligned} g_{\ddot{\nu}n_x}^{[j]} = & \left[-\frac{3}{5} j_1(\varphi) + \frac{2}{5} j_3(\varphi) \right] \sin(\Omega t_j) \\ & - 4 j_2(\varphi) \left(\frac{t_j - t_0}{T} \right) \cos(\Omega t_j) \\ & - 12 j_1(\varphi) \left(\frac{t_j - t_0}{T} \right)^2 \sin(\Omega t_j), \end{aligned} \quad (80d)$$

$$\begin{aligned} g_{\ddot{\nu}n_y}^{[j]} = & \left[\frac{3}{5} j_1(\varphi) - \frac{2}{5} j_3(\varphi) \right] \cos(\Omega t_j) \\ & - 4 j_2(\varphi) \left(\frac{t_j - t_0}{T} \right) \sin(\Omega t_j) \\ & + 12 j_1(\varphi) \left(\frac{t_j - t_0}{T} \right)^2 \cos(\Omega t_j). \end{aligned} \quad (80e)$$

The components $g_{ab}^{[j]}$ of the coherent metric tensor are explicitly independent of the coordinates as mentioned earlier. Therefore, the number of coarse-grid templates $\mathcal{N}_t^{\text{coarse}}$ is also computed as presented by Eq. (53). To analytically estimate the actual value of $\mathcal{N}_t^{\text{coarse}}$ for the two-spindown case, in addition to Eqs. (54) and (55) the following ranges of $\ddot{\nu}$ are assumed to be searched

$$-\pi \frac{T^3 f}{12 \tau_{\min}^2} \lesssim \ddot{\nu} \lesssim \pi \frac{T^3 f}{12 \tau_{\min}^2}. \quad (81)$$

Thus, evaluation of Eq. (53) yields in this case

$$\begin{aligned} \mathcal{N}_t^{\text{coarse}} &= \rho_0 \sqrt{\det g^{[j]}} \int_{\pi T f_{\min}}^{\pi T f_{\max}} d\nu \int_{\mathcal{D}_f} dn_x dn_y \\ &\times \int_{-\frac{\pi T^2 f}{4 \tau_{\min}}}^{\frac{\pi T^2 f}{4 \tau_{\min}}} d\dot{\nu} \int_{-\frac{\pi T^3 f}{12 \tau_{\min}^2}}^{\frac{\pi T^3 f}{12 \tau_{\min}^2}} d\ddot{\nu} \\ &\approx \rho_0 \sqrt{\det g^{[j]}} \frac{\pi^6 T_E^2}{15 \tau_{\min}^3} T^6 (f_{\max}^5 - f_{\min}^5). \quad (82) \end{aligned}$$

The determinant of the coherent metric tensor $g^{[j]}$ for the two-spindown case is obtained accordingly as

$$\begin{aligned} \det g^{[j]} &= \frac{4}{23625} [1 + 375 j_1^2(\varphi) j_2^2(\varphi) + 189 j_1^4(\varphi) \\ &- 252 j_1^3(\varphi) j_3(\varphi) + 84 j_1^2(\varphi) j_3^2(\varphi) \\ &+ 42 j_1(\varphi) j_3(\varphi) - 42 j_0(\varphi) j_1(\varphi) j_3(\varphi) \cos(\varphi) \\ &+ 75 j_1^3(\varphi) \sin(\varphi) / 2 - 14 j_3^2(\varphi) - 10 j_2^2(\varphi) \\ &+ 14 j_0(\varphi) j_3^2(\varphi) \cos(\varphi) - 69 j_1^2(\varphi) \\ &+ 10 j_0(\varphi) j_2^2(\varphi) \cos(\varphi) - 2 j_0(\varphi) \cos(\varphi) \\ &+ 69 j_0(\varphi) j_1^2(\varphi) \cos(\varphi) + j_0^2(\varphi) \cos^2(\varphi) \\ &- j_1(\varphi) \sin(\varphi) + j_0(\varphi) j_1(\varphi) \sin(\varphi) \cos(\varphi)]. \quad (83) \end{aligned}$$

As mentioned earlier, $\det g^{[j]}$ only depends upon φ . To investigate the scaling of $\mathcal{N}_t^{\text{coarse}}$ with the coherent integration time T , Fig. 4 shows $T^6 \sqrt{\det g^{[j]}}$, being a measure for $\mathcal{N}_t^{\text{coarse}}$, versus T . For increasing values of T , $\det g^{[j]}$ converges to the constant value of $4/23625$, since the metric tensor components related to the Earth's spinning motion, n_x and n_y , become approximately constant in this regime as explained earlier in Sec. V A.

Finally, it should be pointed out that choosing $t_0 = t_j = 0$ simplifies the expressions of Eqs. (80), yielding

$$g_{\nu\dot{\nu}}^{[j=0]} = \frac{1}{5}, \quad (84a)$$

$$g_{\dot{\nu}\ddot{\nu}}^{[j=0]} = 0, \quad (84b)$$

$$g_{\nu\ddot{\nu}}^{[j=0]} = \frac{1}{7}, \quad (84c)$$

$$g_{\dot{\nu}n_x}^{[j=0]} = 0, \quad (84d)$$

$$g_{\dot{\nu}n_y}^{[j=0]} = \left[\frac{3}{5} j_1(\varphi) - \frac{2}{5} j_3(\varphi) \right]. \quad (84e)$$

B. Semicoherent metric

The extra components of the semicoherent metric tensor \bar{g} are then obtained via Eq. (40) using Eqs. (80) as

$$\bar{g}_{\nu\dot{\nu}} = \frac{1}{5} + 4 \mu_2, \quad (85a)$$

$$\bar{g}_{\dot{\nu}\ddot{\nu}} = \frac{4}{3} \mu_1 + 16 \mu_3, \quad (85b)$$

$$\bar{g}_{\nu\ddot{\nu}} = \frac{1}{7} + 8 \mu_2 + 48 \mu_4, \quad (85c)$$

$$\begin{aligned} \bar{g}_{\dot{\nu}n_x} &= \left[-\frac{3}{5} j_1(\varphi) + \frac{2}{5} j_3(\varphi) \right] \mu_0^{\text{SIN}} \\ &- 4 j_2(\varphi) \mu_1^{\text{COS}} - 12 j_1(\varphi) \mu_2^{\text{SIN}}, \quad (85d) \end{aligned}$$

$$\begin{aligned} \bar{g}_{\dot{\nu}n_y} &= \left[\frac{3}{5} j_1(\varphi) - \frac{2}{5} j_3(\varphi) \right] \mu_0^{\text{COS}} \\ &- 4 j_2(\varphi) \mu_1^{\text{SIN}} + 12 j_1(\varphi) \mu_2^{\text{COS}}. \quad (85e) \end{aligned}$$

With the approximations of Eqs. (67) used earlier, $\mu_0^{\text{SIN}} \approx 0$, $\mu_0^{\text{COS}} \approx 0$, $\mu_1^{\text{SIN}} \approx 0$, $\mu_1^{\text{COS}} \approx 0$, and the t_0 choice of Eq. (66) the semicoherent metric tensor components in Eqs. (85) take the following form

$$\bar{g}_{\nu\dot{\nu}} = \frac{1}{5} + 4 \hat{\mu}_2, \quad (86a)$$

$$\bar{g}_{\dot{\nu}\ddot{\nu}} \approx 0, \quad (86b)$$

$$\bar{g}_{\nu\ddot{\nu}} = \frac{1}{7} + 8 \hat{\mu}_2 + 48 \hat{\mu}_4, \quad (86c)$$

$$\bar{g}_{\dot{\nu}n_x} \approx -6 j_1(\varphi) \hat{\mu}_2^{\text{COS}} \approx -6 j_1(\varphi) \hat{\mu}_2, \quad (86d)$$

$$\bar{g}_{\dot{\nu}n_y} \approx 6 j_1(\varphi) \hat{\mu}_2^{\text{SIN}} \approx 6 j_1(\varphi) \hat{\mu}_2. \quad (86e)$$

Thus, the full five-dimensional semicoherent metric tensor \bar{g} is obtained as

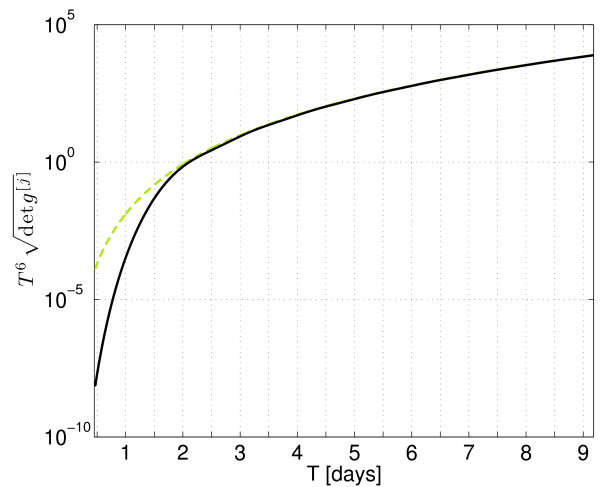


FIG. 4: Dependency of the number of coarse-grid templates $\mathcal{N}_t^{\text{coarse}}$ on the coherent integration time T (segment length) for the two-spindown case. The solid curve shows $T^6 \sqrt{\det g^{[j]}}$, since $\mathcal{N}_t^{\text{coarse}} \propto T^6 \sqrt{\det g^{[j]}}$. The dashed curve shows $T^6 \sqrt{4/23625}$.

$$\bar{g} \approx \begin{pmatrix} \frac{1}{3} & 0 & \frac{1}{5} + 4\hat{\mu}_2 & 0 & 0 \\ 0 & \frac{4}{45} + \frac{16}{3}\hat{\mu}_2 & 0 & 0 & 0 \\ \frac{1}{5} + 4\hat{\mu}_2 & 0 & \frac{1}{7} + 8\hat{\mu}_2 + 48\hat{\mu}_4 & -6j_1(\varphi)\hat{\mu}_2 & 6j_1(\varphi)\hat{\mu}_2 \\ 0 & 0 & -6j_1(\varphi)\hat{\mu}_2 & \frac{R(\varphi)}{2} & 0 \\ 0 & 0 & 6j_1(\varphi)\hat{\mu}_2 & 0 & \frac{R(\varphi)}{2} \end{pmatrix}, \quad (87)$$

where $R(\varphi)$ is given by Eq. (69). The corresponding determinant is obtained as

$$\det \bar{g} \approx \frac{1 + 60\hat{\mu}_2}{23625} 4R^2(\varphi) \times 140 \left[15(\hat{\mu}_4 - \hat{\mu}_2^2) - 45 \frac{j_1^2(\varphi)\hat{\mu}_2^2}{R(\varphi)} + \hat{\mu}_2 \right]. \quad (88)$$

When T is an integer multiple q of one sidereal day, $T = \frac{2\pi}{\Omega}q$, such that $\varphi = \pi q$ and $R(\pi q) = 1$, the determinant of the semicoherent metric tensor takes the form

$$\det \bar{g} \approx \frac{1 + 60\hat{\mu}_2}{675} 16 \left[15(\hat{\mu}_4 - \hat{\mu}_2^2) - \frac{45\hat{\mu}_2^2}{\pi^2 q^2} + \hat{\mu}_2 \right]. \quad (89)$$

C. Parameter-space resolution refinement

The refinement factor for the two-spindown parameter case γ_2 has been defined through Eq. (73) as

$$\gamma_2 = \sqrt{\frac{\det \bar{g}}{\det g^{[j]}}}. \quad (90)$$

Here $g^{[j]}$ and \bar{g} denote the coherent and semicoherent metric tensors, respectively, for the two-spindown parameter case. Substituting $\det g^{[j]}$ by Eq. (83) and $\det \bar{g}$ by Eq. (88) yields

$$\gamma_2 = 2\sqrt{35} \sqrt{1 + 60\hat{\mu}_2} \times \left[15(\hat{\mu}_4 - \hat{\mu}_2^2) - 45 \frac{j_1^2(\varphi)\hat{\mu}_2^2}{R(\varphi)} + \hat{\mu}_2 \right]^{1/2} U(\varphi), \quad (91)$$

where the explicit expression for $U(\varphi)$ can be deduced from Eq. (83) (suppressed for brevity here).

From Eq. (91) the scaling of γ_2 at leading order in N is obtained as $\gamma_2 \propto N^3$, using $\hat{\mu}_4 \propto N^4$ and $\hat{\mu}_2 \propto N^2$. This cubic scaling with N is solely due to the first and second spindown parameters, resulting from the product of possible linear and quadratic spindown tracks in frequency across the segments, which obviously grows as N^3 .

Note that in general, for s spindown parameters, the expected scaling of the refinement factor γ_s with the number of data segments N is given by

$$\gamma_s \propto N^{s(s+1)/2}. \quad (92)$$

This scaling with N is robust and agrees with what can be deduced from the numerical findings of Ref. [16].

D. Illustrative example

To further examine γ_2 , it is instructive to consider again the example data set presented in Sec. VD. Thus, given $t_j = [j - (N + 1)/2]T$ and $t_0 = 0$, the third central moment vanishes, $\hat{\mu}_3 = 0$, and the fourth central moment $\hat{\mu}_4$ is obtained as

$$\hat{\mu}_4 = \frac{N^4}{80} - \frac{N^2}{24} + \frac{7}{240}. \quad (93)$$

Furthermore, it holds

$$\hat{\mu}_4 - \hat{\mu}_2^2 = \frac{N^4}{180} - \frac{N^2}{36} + \frac{1}{45}. \quad (94)$$

Using Eq. (93) along with Eq. (76) the refinement factor γ_2 can be computed as a function of T and N , as illustrated in Fig. 5. For increasing values of T , γ_2 rapidly converges to some constant value for fixed N . In this case, $\det g^{[j]}$ of Eq. (83) is well approximated by $4/23625$ and $\det \bar{g}$ of Eq. (89) by

$$\det \bar{g} \approx \frac{240}{675} (1 + 60\hat{\mu}_2) (\hat{\mu}_4 - \hat{\mu}_2^2). \quad (95)$$

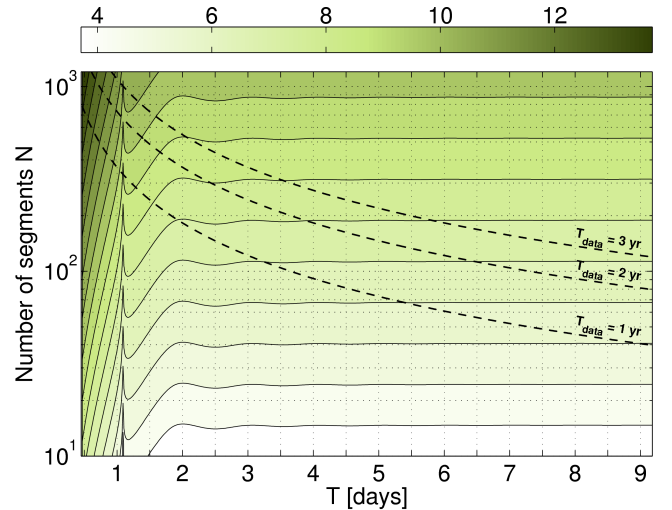


FIG. 5: Refinement factor γ_2 for the two-spindown case. In this plot the color-coded contours show $\log_{10}(\gamma_2)$ as a function of the coherent segment length T and the number of segments N . It has been assumed that there are no gaps between neighboring segments. The dashed lines mark locations of data sets with total time span ($T_{\text{data}} = NT$) of one, two, and three years.

Hence, γ_2 in this case is described by

$$\begin{aligned}\gamma_2 &\approx \sqrt{2100 (1 + 60 \hat{\mu}_2) (\hat{\mu}_4 - \hat{\mu}_2^2)} \\ &\approx \gamma_1 \sqrt{(35 N^4 - 175 N^2 + 140)/3}.\end{aligned}\quad (96)$$

where Eqs. (76) and (94) have been used. Thus, the anticipated scaling at leading order in N is recovered: $\gamma_2 \propto N^3$.

VII. CONCLUSION

A formalism has been presented for the parameter-space metric of semicoherent CW searches, where the data are divided into segments that are coherently analyzed and subsequently combined incoherently. By using new coordinates on parameter space, the first fully analytical semicoherent metric for broadband all-sky CW surveys has been derived. Additionally, in the new coordinates the components of both the coherent and the semicoherent metric tensor are constant, being explicitly independent of the coordinates. This entails great convenience regarding practical aspects of semicoherent CW searches.

Explicit analytic expressions of the semicoherent metric tensor components have been obtained for two typical search parameter spaces of current practical interest. First, the one-spindown case has been considered, restricting to linear frequency drifts with time as done in many current all-sky searches. Second, the semicoherent metric also has been calculated and examined for the two-spindown case, where additionally quadratic changes in frequency are taken into account.

Analytic signal template counting formulas have been provided for the coherent stage (coarse grid) as well as for the incoherent combination step (fine grid). In this respect, a

useful quantity, called the *refinement factor*, has been introduced as the ratio of the number of fine-grid and coarse-grid templates. Thus, the refinement factor describes (coordinate independently) the additional parameter-space metric resolution gained from the combination of segments. Moreover, the scaling of the refinement factor with the number of segments has been found to be predominantly determined solely by the spindown parameters.

The present results also embed the case of directed semicoherent searches, where the sky position is known and hence is not a search parameter. Thereby, the search parameter space consists only of frequency and spindown parameters. The corresponding semicoherent metric tensor components are identical to ones derived here. The resulting scalings of the refinement factor with the number of segments also hold, since governed by the spindown parameters as described above.

The formalism presented in this paper assumes segments that are very short compared to one year. The Earth's orbital motion then can be described by a low-order Taylor expansion, and therefore be modeled by changes in frequency and frequency derivatives. In the future, however, increased computing power might allow one to use segments substantially longer than a few days and hence issues remain to be explored in such circumstances.

VIII. ACKNOWLEDGMENTS

I am indebted to Bruce Allen, Reinhard Prix, and Chris Messenger for very useful discussions and helpful comments on this work. I also thank Miroslav Shaltev for corrections of the manuscript. I gratefully acknowledge the support of the Max-Planck-Society. This document has been assigned LIGO Document Number LIGO-P1000006-v4.

-
- [1] B. J. Owen, L. Lindblom, C. Cutler, B. F. Schutz, A. Vecchio, and N. Andersson, *Phys. Rev. D* **58**, 084020 (1998).
 - [2] G. Ushomirsky, C. Cutler, and L. Bildsten, *Mon. Not. Roy. Astron. Soc.* **319**, 902 (2000).
 - [3] C. Cutler, *Phys. Rev. D* **66**, 084025 (2002).
 - [4] D. I. Jones and N. Andersson, *Mon. Not. Roy. Astron. Soc.* **331**, 203 (2002).
 - [5] B. J. Owen, *Phys. Rev. Lett.* **95**, 211101 (2005).
 - [6] B. Abbott et al. (The LIGO Scientific Collaboration), *Rep. Prog. Phys.* **72**, 076901 (2009).
 - [7] B. Abbott et al. (The LIGO Scientific Collaboration), *Phys. Rev. D* **77**, 022001 (2008).
 - [8] B. Abbott et al. (The LIGO Scientific Collaboration), *Phys. Rev. D* **79**, 022001 (2009).
 - [9] B. Abbott et al. (LIGO Scientific Collaboration), *Phys. Rev. D* **80**, 042003 (2009).
 - [10] <http://einstein.phys.uwm.edu/>.
 - [11] B. Abbott et al. (The LIGO Scientific Collaboration), *The Astrophysical Journal Letters* **683**, L45 (2008).
 - [12] B. Abbott et al. (The LIGO Scientific Collaboration), *Phys. Rev. Lett.* **102**, 111102 (2009).
 - [13] P. Jaranowski, A. Królak, and B. F. Schutz, *Phys. Rev. D* **58**, 063001 (1998).
 - [14] C. Cutler and B. F. Schutz, *Phys. Rev. D* **72**, 063006 (2005).
 - [15] P. R. Brady, T. Creighton, C. Cutler, and B. F. Schutz, *Phys. Rev. D* **57**, 2101 (1998).
 - [16] P. R. Brady and T. Creighton, *Phys. Rev. D* **61**, 082001 (2000).
 - [17] C. Cutler, I. Gholami, and B. Krishnan, *Phys. Rev. D* **72**, 042004 (2005).
 - [18] B. Krishnan, A. M. Sintes, M. A. Papa, B. F. Schutz, S. Frasca, and C. Palomba, *Phys. Rev. D* **70**, 082001 (2004).
 - [19] H. J. Pletsch and B. Allen, *Phys. Rev. Lett.* **103**, 181102 (2009).
 - [20] R. Balasubramanian, B. S. Sathyaprakash, and S. V. Dhurandhar, *Phys. Rev. D* **53**, 3033 (1996).
 - [21] B. J. Owen, *Phys. Rev. D* **53**, 6749 (1996).
 - [22] I. Jones, B. J. Owen and D. Whitbeck, LIGO Document T0900500-v1, 2005, available at <https://dcc.ligo.org/>.
 - [23] R. Prix, *Phys. Rev. D* **75**, 023004 (2007).
 - [24] S. Dhurandhar, B. Krishnan, H. Mukhopadhyay, and J. T. Whelan, *Phys. Rev. D* **77**, 082001 (2008).
 - [25] A. L. Watts, B. Krishnan, L. Bildsten, and B. F. Schutz, *Mon. Not. Roy. Astron. Soc.* **389**, 839 (2008).
 - [26] H. J. Pletsch, *Phys. Rev. D* **78**, 102005 (2008).
 - [27] R. Prix and Y. Itoh, *Class. Quant. Grav.* **22**, S1003 (2005).

-
- [28] P. Jaranowski and A. Królak, Phys. Rev. D **59**, 063003 (1999).
[29] P. Jaranowski and A. Królak, Phys. Rev. D **61**, 062001 (2000).
[30] P. Jaranowski and A. Królak, Living Rev. Relativity **8**, 3 (2005),
<http://www.livingreviews.org/lrr-2005-3/>.
[31] P. Astone, K. M. Borkowski, P. Jaranowski, and A. Królak,
Phys. Rev. D **65**, 042003 (2002).
[32] P. Astone, K. M. Borkowski, P. Jaranowski, M. Pietka, and
A. Królak, Phys. Rev. D **82**, 022005 (2010).
[33] P. Jaranowski and A. Królak, *Analysis of gravitational-wave
data* (Cambridge University Press, Cambridge, 2009).
[34] R. Prix, Class. Quant. Grav. **24**, S481 (2007).
[35] C. Messenger, R. Prix, and M. A. Papa, Phys. Rev. D **79**,
104017 (2009).
[36] G. M. Manca and M. Vallisneri, Phys. Rev. D **81**, 024004
(2010).
[37] M. Abramowitz and I. A. Stegun, *Handbook of Mathematical
Functions with Formulas, Graphs, and Mathematical Tables*
(Dover, New York, 1964).
[38] K. Wette et al., Class. Quant. Grav. **25**, 235011 (2008).